Journal of Applied Mathematics and Physics, 2014, 2, 77-87
Published Online April 2014 in SciRes. http://www.scirp.org/journal/jamp
http://dx.doi.org/10.4236/jamp.2014.25011

Scientific Research

Magnetic Properties and Hyperfine Interactions in M-Type $BaFe_{12-2x}Mo_xZn_xO_{19}$ Hexaferrites

Sami H. Mahmood[1*], Ghada H. Dushaq[1], Ibrahim Bsoul[2], Mufeed Awawdeh[3], Hassan K. Juwhari[1], Bashar I. Lahlouh[1], Murad A. AlDamen[4]

[1]Physics Department, The University of Jordan, Amman, Jordan
[2]Physics Department, Al al-Bayt University, Mafraq, Jordan
[3]Physics department, Yarmouk University, Irbid, Jordan
[4]Chemistry Department, The University of Jordan, Amman, Jordan
Email: [*]s.mahmood@ju.edu.jo, ghb1905@yahoo.com, ibrahimbsoul@yahoo.com, amufeed@yu.edu.jo, h.juhari@ju.edu.jo, bashar_lahlouh@ju.edu.jo, maldamen@ju.edu.jo

Received January 2014

Abstract

A series of M-Type barium hexaferrites with the general composition $BaFe_{12-2x}Mo_xZn_xO_{19}$ were synthesized at 1100˚C by a simple wet chemical mixture route. The properties of the prepared samples were examined by X-ray diffraction, scanning electron microscopy, vibrating sample magnetometry, and Mössbauer spectroscopy. The diffraction patterns for all samples were found to agree well with the standard pattern of $BaFe_{12}O_{19}$ hexaferrite with no extraneous diffraction peaks. The products formed as well crystallized hexagonal platelet-like particles while the EDS measurements revealed the stoichiometric cationic ratios of the prepared samples. The spectral variations elucidated by Mössbauer spectroscopy were utilized to determine the different cation preferential site occupations as a function of *x*. Finally, the saturation magnetizations, magnetic anisotropies, and the anisotropy fields, determined from the magnetic measurements, showed consistency with the relative subspectral Mössbauer intensities and the single ion model for the anisotropy constant.

Keywords

Mössbauer Spectroscopy Magnetic Properties, Hysteresis, Crystal Field, Sintering; Magnetic Materials

1. Introduction

M-type barium hexaferrite with the formula $BaFe_{12}O_{19}$ belongs to a class of hexagonal ferrites with relatively high saturation magnetization and tunable coercive fields. The magnetic properties, in addition to corrosion re-

[*]Corresponding author.

How to cite this paper: Mahmood, S.H., *et al.* (2014) Magnetic Properties and Hyperfine Interactions in M-Type $BaFe_{12-2x}Mo_xZn_xO_{19}$ Hexaferrites. *Journal of Applied Mathematics and Physics*, **2**, 77-87.
http://dx.doi.org/10.4236/jamp.2014.25011

sistance and low production cost, make these ferrites of great commercial and technological importance [1,2]. The great current scientific and technological interest in M-type ferrites was driven by their potential for a wide range of applications in permanent magnets, high density magnetic recording and data storage media, microwave absorption and next-generation microwave devices [1-8].

The unit cell of BaM consists of two spinel (S) blocks and two hexagonal (R) blocks with a stacking sequence RSR*S*, where R* and S* are rotated by 180˚ around the hexagonal *c*-axis. The unit cell contains two formula units, where the Ba^{2+} ion replaces an oxygen ion substitutionally in the middle layer of the R block, and the ferric ions reside in the three octahedral (12*k*, 4f_2 and 2*a*) sites, the tetrahedral (4f_1)site and the trigonalbi-pyramidal (2*b*) site. The spin orientations of the Fe^{3+} ions in the 2*a*, 2*b*, and 12*k* sites are parallel (spin-up sublattices), and the spins of the ions in the 4f_1 and 4f_2 sites are parallel to each other and in opposite direction to spin-up sublattices (spin-down sublattices). The prefix number associated with the symbol for each site is the number of metallic ions per unit cell occupying that site. Accordingly, the magnetic moment per formula can be expressed as follows:

$$m = 6m_{12k} + m_{2b} + m_{2a} - 2m_{4f1} - 2m_{4f2} \quad (1)$$

The magnetocrystalline anisotropy in these ferrites arises from the coupling of the spins of Fe^{3+} at different sites. The contributions of the various sites to the magnetic anisotropy was calculated on the basis of single-ion model [9], and it was shown that iron ions at 2*b* sites have the largest positive contribution, and those at 12*k* sites have a relatively weak negative contribution, while the remaining sites have a relatively weak postive contribution. Accordingly, the magnetic properties of the hexaferrites were modified by substituting Fe^{3+} ions by a trivalent metal ion such as Al, Ga, In, Sc, As, Cr [10-16], or combinations of a tetravalent ion such as Ti^{4+}, Ru^{4+}, Zr^{4+}, or Sn^{4+} with a divalent ion such as Mn^{2+}, Ni^{2+}, Mg^{2+}, Co^{2+}, Zn^{2+}, Ti^{2+} or Sn^{2+} [4,17-22]. The structural and physical properties of the fabricated hexaferrite powders were found to be affected by the physical or chemical preparation method, as well as the experimental conditions such as stoichiometry, heat treatment, and binder additives [11,17,18,23-30].

Among other techniques used to characterize the hexaferrites, magnetic measurements and Mössbauer spectroscopy were extensively used in the last five decades. While the magnetic measurements give some sort of an average of the magnetic propertie over the whole sample investigated, ^{57}Fe Mössbauer spectroscopy gives information on the local chemical and structural environment, in addition to the valence state of the iron ions in the lattice. This valuable information was used to explain the magnetic behavior and the magnetic interactions in barium and strontium based hexaferrites [5,11,31-34].

The Mössbauer data available in the literature for pure barium hexaferrites at room temperature demonstrated a wide range of variability in the hyperfine parameters of the hexaferrites. Although the parameters for the 12*k* and 2*b* components are clearly distingushable from the remaining components due to the high rlative intensity of the first and the large quadrupole splitting of the second, clear disagreements were found even on the parameters of these components. Hyperfine fields for the 4$f_2$were reported between about 512 kOe [35,36] and 528 kOe [37], which differ by more than the usual experimental uncertainty of 5 kOe. Furthermore, the intensity for this component (with a theoretical value of 50%) was reported between 46.4% [38] and 50.6% [35,36]. While on the other hand, values of the quadrupole splitting for the 2b component were reported between as low as 2.03 mm/s [39] and as high as 2.30 mm/s [40], with a variation significantly higher than the usually accepted experimental uncertainty of 0.02 mm/s. The intensity for this component was reported between 3.7% [39] and 6.7% [35], and the isomer shift between 0.18 mm/s [35] and 0.32 mm/s [41]. The variations in the hyperfine parameters and relative intensity for the 2*b* component could be due to the low intensity of this component and the complexity of the spectrum. Also, significant variations in the hyperfine parameters and relative intensities for the 4f_2, 2*a*, and 4f_1 components were reported in the literature [13,35,36,40,42]. Such variations, we believe, arise from the similarity of the parameters for these components which lead to the mixing of the corresponding subspectra and the difficulty to resolve the low intensity 2*a* component. The proximity of the parameters for these components lead the majority of investigators to consider mixing of the 2*a*-4f_1 components into one subspectrum and few others to consider 2*a*-4f_2 [36,39] mixing in their fitting procedure.

In a recent study [43], the magnetic properties and hyperfine parameters were reported for the system $BaFe_{11.6}Mo_xZn_{0.4-x}O_{19}$ (x =0.1, 0.2, 0.4) with the focus on the distribution of Mo ions with different valencies (Mo^{4+} and Mo^{6+}) and its effects on the magnetic properties. In this study the magnetic properties and hyperfine interactions for the system $BaFe_{12-2x}Mo_xZn_xO_{19}$ (x = 0, 0.05, 0.1, 0.15, 0.2, 0.3) prepared by wet chemical mix-

ture method were investigated. The structural properties of the samples were investigated by powder x-ray diffraction, and the morphology of the particles and the stoichiometry of the samples were checked by scanning electron microscopy (SEM) equipped with energy dispersive x-ray spectroscopy (EDS) facility. Also, the effects of $Mo^{4+}Zn^{2+}$ concentration on the cationic distribution and the magnetocrystalline anisotropy were evaluated.

2. Experimental

The precursors of $BaFe_{12-2x}Mo_xZn_{0.4-x}O_{19}$($x$ = 0.00, 0.05, 0.10, 0.15, 0.20, 0.30) were synthesized by the wet chemical mixture method described earlier [43]. The required molarities of at least 99% pure Fe_2O_3, $BaCO_3$, ZnO and MoO_3 were added to distilled water and mixed together in a beaker with continuous stirring on a magnetic stirrer. The mixture was refluxed at 150˚C for 24 hrs, filtered and then left to dry in air. The resulting powders were pressed into pellets 1.5 cm in diameter, and sintered in air atmosphere at 1100˚C for 2 hr. The Fe/Ba ratio was 11 to avoid the persistence of α-Fe_2O_3 secondary phase. Samples containing small amounts of $BaFe_2O_4$ intermediate phase were sintered again at 1100˚C for better reaction and elimination of intermediate phases.

The structure of the samples and the unit cell volumes were determined from XRD patterns using Philips X'Pert PRO X-ray diffractometer (PW3040/60) with CuK_α radiation (λ = 1.54 Å).The patterns were recorded in the angular range 15˚ < 2θ < 75˚ with scanning step of 0.017˚. The morphology of the particles and the stoichiometry of the prepared samples were examined using scanning electron microscope (SEM FEI-Inspect F50/FEG) equipped with energy dispersive X-ray analysis (EDS) facility.

^{57}Fe Mössbauer spectra were recorded using a standard constant acceleration Mössbauer spectrometer with a ^{57}Co/Cr source. The spectra were calibrated using iron metal spectrum at room temperature and the experimental spectra were fitted using routines based on least squares analysis.

Room temperature magnetic measurements were obtained using a vibrating sample magnetometer (VSM MicroMag 3900, Princeton Measurements Corporation), with a maximum applied field of 10 kOe. The needle-shaped samples for magnetic measurements were cut from the sintered sample disks.

3. Results and Discussion

3.1. X-Ray Diffraction

Figure 1 shows representative XRD patterns together with the standard pattern for comparison. XRD patterns for all samples show $BaFe_{12}O_{19}$ M-type hexaferrite phase with lattice parameters consistent with the standard pattern (JCPDS 00-043-0002). The lattice parameters are a = 5.887 ± 0.002 Å and c = 23.17 ± 0.005 Å, and the cell volume is 695.9 ± 0.5 Å^3. The X-ray density increases from 5.30 g/cm^3 for the sample with x = 0.00 to 5.40 g/cm^3 for that with x = 0.3.

The average crystallite sizes for the samples were calculated from the positions of the (107) and (114) peaks using the well-known Scherrer formula [44]:

$$D = k\lambda / \beta \cos\theta. \quad (2)$$

Here D is the crystallite size, k is the Scherrer constant, λ is the wavelength of radiation (1.54 Å), β is the peak width at half maximum, and θ is the peak position. The average crystallite sizes of all samples were found to decrease slightly from 52 nm for the sample with x = 0.00 to 45 nm for that with x = 0.30.

3.2. Scanning Electron Microscopy

The morphology and average particle size, and the stoichiometry of the samples under investigation were examined using SEM imaging and EDS. **Figure 2** shows representative images for the samples with x = 0.15 and x = 0.20. Other images were investigated for statistical purposes. We noticed that the prepared samples consisted mainly of hexagonal platelet-like particles with diameters ranging from about 100nm to about 500nm for low Mo-Zn concentrations, and platelets with diameters larger than 1 μm were observed at higher concentrations. From these observations it seems that the Mo-Zn cations in the lattice improve the inter-particle connectivity and leads to crystal growth.

Energy dispersive spectra for the samples were examined and the atomic ratios of the constituents were obtained. The spectra were collected by focusing the electron beam at one particle at a time. Weak peaks corres-

ponding to Zn and Mo were observed, indicating the incorporation of the metal ions in the hexaferrite lattice (see for example **Figure 3** for the samples with x = 0.20). The relative peak intensities derived from this spectrum correspond to atomic concentrations of (0.97 ± 0.13) Ba, (10.6 ± 0.6) Fe, (0.10 ± 0.10) Zn, and (0.21 ± 0.10) Mo. These atomic concentrations reflect the stoichiometric composition, and correspond to Fe/Ba ratio within 10% of the stoichiometric ratio. Similar results were obtained for the other samples.

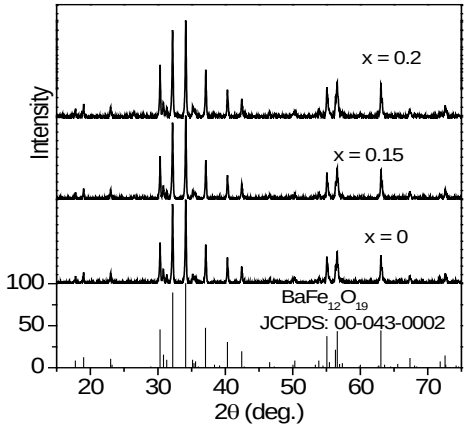

Figure 1. XRD patterns for$BaFe_{12-2x}Mo_xZn_xO_{19}$ (x = 0.00, 0.15, 0.20) samples. The standard pattern for M-type barium hexaferrite (file no: 043-0002) is included for comparison.

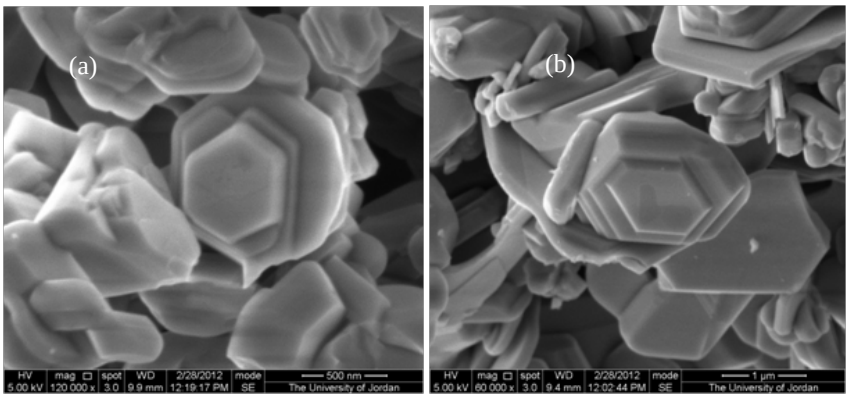

Figure 2. SEM micrographs for (a) the sample with x = 0.15, and (b) the sample with x = 0.2.

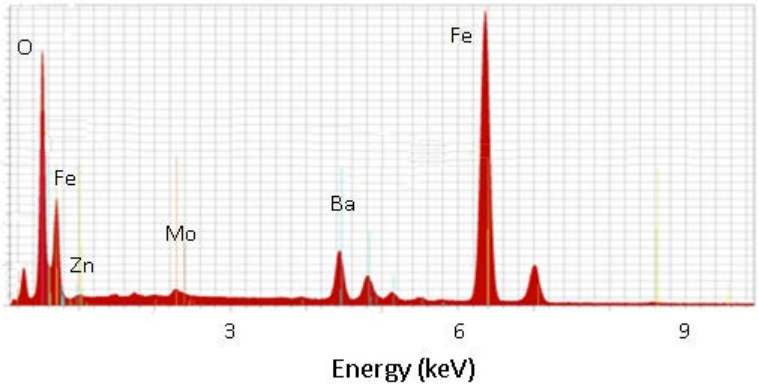

Figure 3. Energy dispersive spectrum for the sample with x = 0.20.

3.3. Mössbauer Spectroscopy

Mössbauer spectra of all samples are shown in **Figure 4**. Each spectrum was fitted with magnetically split sextet components corresponding to iron ions in the five crystallographic sites $4f_2$, $4f_1$, $2a$, $12k$, $2b$ of the BaM hexaferrite structure, and the fitting parameters are listed in **Table 1**. The hyperfine parameters for pure sample are in good agreement with the results of previous studies [40,41]. The observed deviations of the relative intensities form the theoretical values of 16.7%:8.3%:16.7%, 50.0%:8.3%, respectively, could be due to differences in Mössbauer Lamb factors for the different sites, leading to different absorption efficiencies. Assuming that the absorption efficiencies do not vary with the low level of substitution in our samples, the number of Fe^{3+} ions at each site per formula was derived by multiplying the corresponding relative intensity by the number of Fe ions in the molecule. **Figure 5** shows the site multiplicity for the $2b$ and $12k$ sites (normalized to their values for the un-substituted sample). It is well known that the substitution of non-magnetic ions at $2b$ sites reduces the hyperfine fields at neighboring $12k$ and $4f_2$ sites [15]. As a consequence, the intensities of the $2a$ and $4f_1$ components would increase and spectral line-width of the $12k$ component would enhance for small amounts of substituents (as observed in the sample with $x = 0.05$, where the inner lines for the $12k$ component increases from 0.27 mm/s to 0.32 mm/s). For higher concentrations of the substituents, the $12k$ component could split into two components, with the lower field component ($12k_1$) corresponding to those $12k$ sites neighboring substituted sites.

Further, the substitution at $4f_1$ site (which is the preferred site for Zn^{2+} ions) perturbs the $2a$ and $12k$ sites, which results in the reduction in hyperfine fields for the sites neighboring Zn^{2+} ions. As a consequence, the $12k_1$ component appears at higher concentration levels. The splitting of the $12k$ component was observed in other hexaferrite systems with some kinds of substituents for Fe ions [34,43,45,46]. The data shown in **Table 1** (and **Figure 5**) demonstrate preference for substitution at $2b$, $12k$ and $4f_2$ sites for low x values. Since ions with high valence states energetically favor octahedral sites, we can assign the drop in relative intensity for the $2b$ spectral component to partial substitution of Zn^{2+} ions at $2b$ sites in this concentration region, and the drop in the relative intensities for the $12k$ and $4f_2$ components to substitution of Mo^{4+} ions at these sites. It is also observed that as x increases from 0.05 to 0.15 the $2b$ and $12k$ sites get less substituted, where Zn^{2+} starts partially entering $4f_1$ site and Mo^{4+} partially occupying other octahedral sites ($4f_2$ and $2a$). For the samples with $x = 0.2$ and 0.3 the $2b$ site is only slightly occupied, while substitution of the $12k$ site becomes evident. However, the overlap of the $2a$, $4f_1$

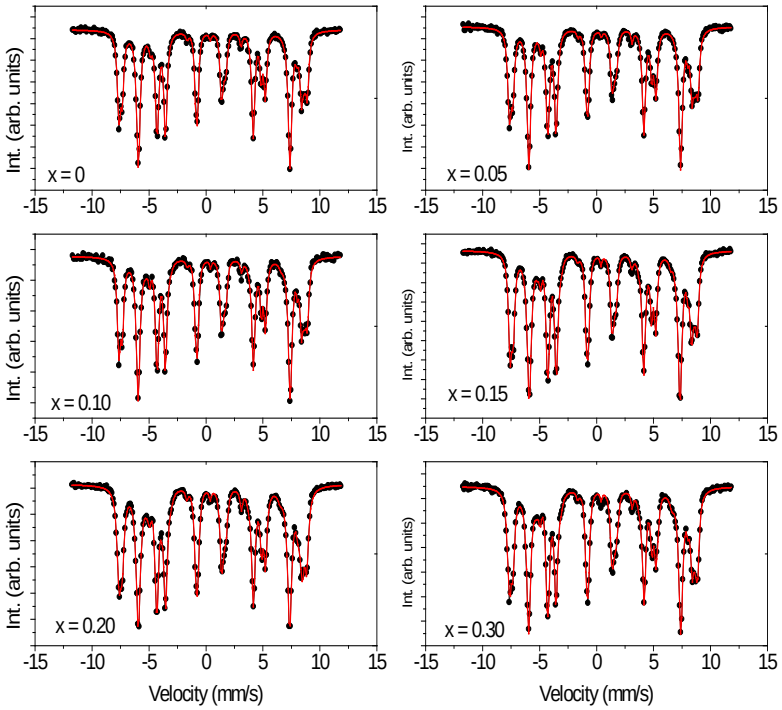

Figure 4. Mössbauer spectra for the $BaFe_{12-2x}Mo_xZn_xO_{19}$ samples (filled circles) together with the theoretical spectrum obtained from the fitting (continuous line).

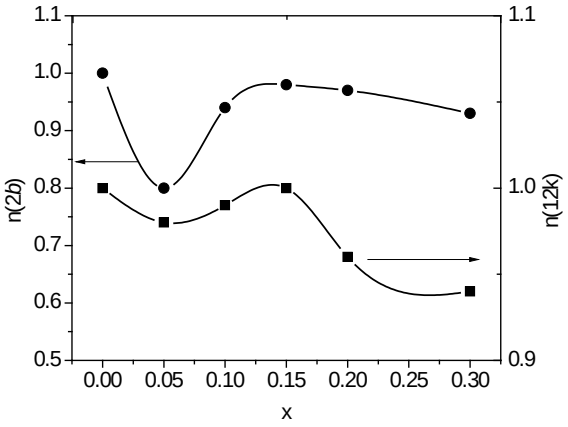

Figure 5. Normalized 2*b* and 12*k* site multiplicities derived from the relative component intensities of Mössbauer spectra for $BaFe_{12-2x}Mo_xZn_xO_{19}$samples.

Table 1. The hyperfine (B_{hf}) fields [kOe], center shifts (*CS*) [mm/s], quadrupole splittings (*QQ*)[mm/s], and percentage relative intensities (*I*) of the components of the spectra.

Parameter	Site	0.00	0.05	0.10	0.15	0.20	0.30
B_{hf1}	$4f_2$	517	517	517	515	517	517
B_{hf2}	2*a*	511	512	511	508	498	515
B_{hf3}	$4f_1$	493	493	493	491	495	493
B_{hf4}	12*k*	417	417	418	415	416	418
B_{hf5}	2*b*	403	405	407	405	407	406
B_{hf6}	$12k_1$	-	-	372	366	370	372
CS_1		0.38	0.38	0.38	0.38	0.38	0.38
CS_2		0.37	0.36	0.37	0.39	0.53	0.38
CS_3		0.27	0.27	0.27	0.27	0.26	0.28
CS_4		0.37	0.37	0.37	0.36	0.36	0.37
CS_5		0.32	0.32	0.31	0.31	0.30	0.31
CS_6		-	-	0.37	0.34	0.33	0.36
QQ_1		0.23	0.25	0.23	0.21	0.15	0.21
QQ_2		0.07	0.06	0.06	0.07	0.06	0.14
QQ_3		0.22	0.22	0.22	0.21	0.19	0.21
QQ_4		0.42	0.42	0.42	0.40	0.39	0.41
QQ_5		2.20	2.17	2.17	2.19	2.20	2.16
QQ_6		-	-	0.34	0.34	0.35	0.35
I_1		16.9	16.1	16.5	17.3	17.3	17.7
I_2		10.7	11.9	10.9	6.8	4.1	10.3
I_3		16.8	17.8	16.8	18.9	23.0	17.2
I_4		50.4	50.0	48.7	49.6	47.3	46.2
I_5		5.1	4.1	4.9	5.1	5.3	5.0
I_6		-	-	2.1	2.3	3.0	3.6

and $4f_2$ components due to perturbation induced by the substituents make it difficult to consider their hyperfine parameters with high confidence. Thus it suffices here to observe the general behavior of variations of the relative intensities to explain the magnetic data, keeping in mind the preferential site occupation of the different cations.

3.4. Magnetic Measurements

The hysteresis loops for all samples are shown in **Figure 6**, where σ is the specific magnetization per gram sample. It is obvious that saturation was not achieved by applying fields up to 10 kOe. The magnetization in the high-field region is dominated by domain rotation, and the magnetization is given by the law of approach to saturation [47]:

$$M = M_s\left(1 - A/H - B/H^2\right) + \chi H \tag{3}$$

Here χH is the forced magnetization term, M_s is the spontaneous saturation magnetization of the domains per unit volume, A is a constant representing the contributions of inclusions and microstress, and B represents the contribution of magnetocrystalline anisotropy. For hexagonal crystals we have:

Here χH is the forced magnetization term, M_s is the spontaneous saturation magnetization of the domains per unit volume, A is a constant representing the contributions of inclusions and microstress, and B represents the contribution of magnetocrystalline anisotropy. For hexagonal crystals we have:

$$B = H_a^{\,2}/15\,. \tag{4}$$

$$H_a = 2K_1/M_s\,. \tag{5}$$

where H_a is the anisotropy field and K_1 is the first anisotropy constant.

A plot of σ vs. $1/H^2$ in the field region 8 kOe < H < 10 kOe for each sample gave a straight line, the intercept of which determined the saturation magnetization for the sample. The slope of the straight line was used to determine the anisotropy field and the first anisotropy constant according to Equations (4) and (5). **Figure 7** shows the obtained saturation magnetizations for the samples, as well as the coercivity, determined directly from the hysteresis loops. The observed saturation magnetization is higher than that reported previously for BaM ferrites prepared by other techniques [26,27]. In our system, the saturation magnetization increases initially with x as a result of the increased level of substitution of Zn^{2+} ions at $4f_1$ and Mo^{4+} ions at $4f_2$ spin-down sites, and peaks at x = 0.15. The drop in saturation magnetization at higher x values results from the increased substitution of Mo^{4+} ions at 12k sites at the expense of $4f_2$ sites. This is consistent with Mössbauer intensities which indicated that the populations of the $4f_2$ sites by Fe^{3+} ions for the samples with x = 0.2 and 0.3 were almost equal to that for the pure sample, while the population of the 12k sites decreased appreciably. The saturation magnetization behavior for these two samples was dictated by the competition between the tendency to increase due to the increased concentration of Zn^{2+} ions in $4f_1$ spin-down site, and the tendency to decrease due to the increased concentration of Mo^{4+} in 12k spin-up site.

Figure 8 shows the anisotropy fields and the anisotropy constants for the samples. The slight decrease in the anisotropy constant $K_1$for x = 0.05 is consistent with Mössbauer relative intensities discussed above. The single-ion model can be used to calculate the anisotropy constants of our samples based on the contributions of the various sites [9] and the relative populations of these sites as derived from Mössbauer relative intensities. Assuming random distribution of Mo^{4+} ions at 12k and $4f_2$ sites and Zn^{2+} ions occupying 2b sites in the sample with x = 0.05 the calculated anisotropy constant is only 2% smaller than that for the pure sample, which is in good agreement with the value obtained from our magnetic data (2% decrease in H_a and 1.5% decrease in K_1). The more significant drop in the anisotropy field for this sample is a consequence of the inverse dependence of this parameter on the saturation magnetization. A similar behavior with a more significant relative decrease is observed in the coercivity behavior. This can be explained by the dependence of the coercive field on the saturation magnetization. According to Stoner-Wohlfarth model for the random assembly of platelet-like particles with crystal anisotropy easy axis parallel to the c-axis and shape anisotropy easy axis in plane the coercive field is given by:

$$H_c = 0.48\left(H_a - N_d M_s\right). \tag{6}$$

where N_d is the demagnetization factor.

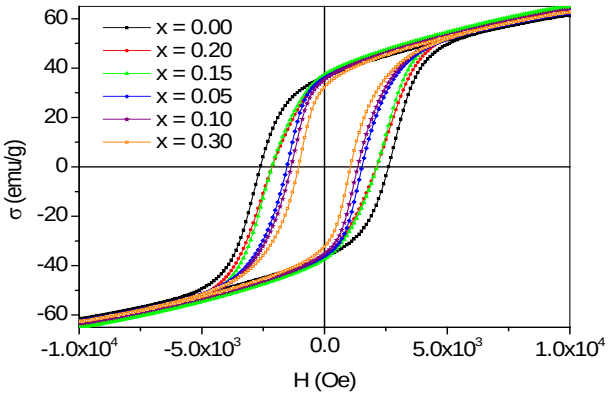

Figure 6. Hysteresis loops for $BaFe_{12-2x}Mo_xZn_xO_{19}$ samples.

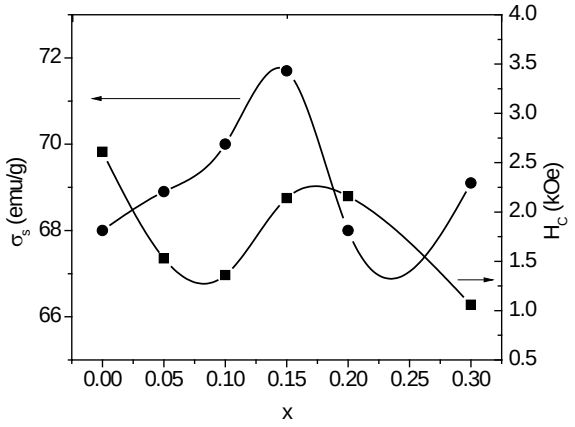

Figure 7. Saturation magnetization and coercivity as a function of *x*.

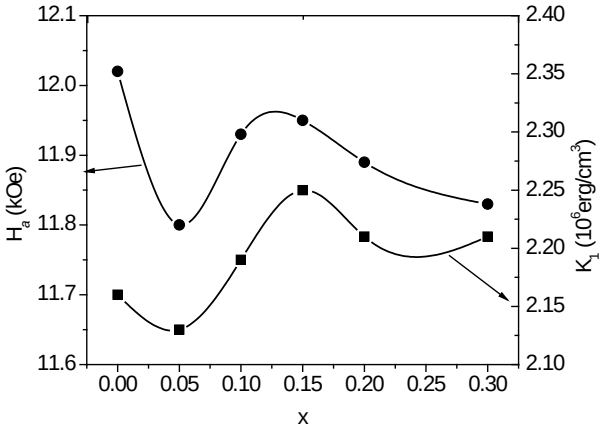

Figure 8. The magnetic anisotropy field and the first anisotropy constant as a function of *x*.

For the sample with $x = 0.05$, the anisotropy constant decreases and the saturation magnetization increases, both effects leading to a decrease in coercivity, which is demonstrated by the significant drop in the coercivity for this sample. For the samples with higher $x = 0.10$ and 0.15 both the saturation magnetization and the anisotropy constant increase, leading to competition between these two effects, and resulting in an initial decrease and then an increase in coercivity. The coercivities for these two samples are still below that for the pure sample, in-

dicating that the effect of the rise in saturation magnetization is dominant in these two samples. For $x = 0.20$, both the anisotropy constant and the saturation magnetization decrease, resulting also in competition between the two effects. Also, the weakening of the super exchange interactions induced by the reduction of the spin-down and spin-up sublattices could play a role in reducing the anisotropy field. Competition between these factors appears to have the same effect on the coercivity as for the sample with $x = 0.15$. The further decrease in coercivity for the sample with $x = 0.30$ could be partially associated with the increase in saturation magnetization with respect to the sample with $x = 0.20$, and partially due to the further reduction in the strength of the superexchange interactions as demonstrated by the reduction in the anisotropy field. The reduced remnant magnetization (σ_r/σ_s) for samples with $0.0 \leq x \leq 0.2$ fall between 0.47 and 0.51, indicating that these samples consist of single domain particles. However, the reduced remanence for the sample with $x = 0.3$ is 0.44, which could indicate the presence of a significant fraction of multidomain particles in this sample. These multidomain particles could also be partially responsible for the observed significant decrease in coercivity.

4. Conclusion

The simple wet chemical mixture method used to prepare $BaFe_{12-2x}Mo_xZn_xO_{19}$ hexaferrite precursors gave samples with relatively high saturation magnetization (68 - 72 emu/g) and low coercivity (1.1 - 2.6 kOe). These magnetic parameters are suitable for applications in high density magnetic recording. The partial substitution of Fe^{3+} ions lead to a redistribution of the ions at the various sites of the hexaferrite lattice, and resulted in changes of the magnetic properties consistent with the relative intensities of Mössbauer sub-spectra.

Acknowledgements

This work was supported by a generous grant from the Deanship of Scientific research at the University of Jordan under contract number 1404.

References

[1] Pullar, R.C. (2012) *Progress in Materials Science*, **57**, 1191. http://dx.doi.org/10.1016/j.pmatsci.2012.04.001

[2] Özgür, U., Alivov, Y. and Morkoç, H.J. (2009) *Journal of Materials Science*: *Materials in Electronics*, **20**, 789. http://dx.doi.org/10.1007/s10854-009-9923-2

[3] Qiu, J., Lan, L., Zhang, H. and Gu, M. (2006) *Materials Science and Engineering*: *B*, **133**, 191. http://dx.doi.org/10.1016/j.mseb.2006.06.049

[4] Ghasemi, A. and Morisako, A. (2008) *Journal of Alloys and Compounds*, **456**, 485. http://dx.doi.org/10.1016/j.jallcom.2007.02.101

[5] Ghasemi, A., Hossienpour, A., Morisako, A., Liu, X. and Ashrafizadeh, A. (2008) *Materials & Design*, **29**, 112. http://dx.doi.org/10.1016/j.matdes.2006.11.019

[6] Dursun, S., Topkaya, R., Akdogan, N. and Alkoy, S. (2012) *Ceramics International*, **38**, 3801.

[7] http://dx.doi.org/10.1016/j.ceramint.2012.01.028

[8] Wise, A.T., Rocks J. Laughlin, D.E., McHenry, M.E., Yoon, S.D., Vittoria, C. and Harris, V.G. (2011) *Journal of Applied Physics*, **109**, 07E535.

[9] Zhang, W., Bai, Y., Han, X., Wang, L., Lu, X. and Qiao, L. (2013) *Journal of Alloys and Compounds*, **546**, 234. http://dx.doi.org/10.1016/j.jallcom.2012.08.029

[10] Xu, Y., Yang, G.L., Chu, A.P. and Zhai, H.R. (1990) *Physica Status Solidi* (*B*), **157**, 685. http://dx.doi.org/10.1002/pssb.2221570221

[11] Awawdeh, M., Bsoul, I. and Mahmood, S.H. (2014) *Journal of Alloys and Compounds*, **585**, 465. http://dx.doi.org/10.1016/j.jallcom.2013.09.174

[12] Bsoul, I. and Mahmood, S.H. (2010) *Journal of Alloys and Compounds*, **489**, 110. http://dx.doi.org/10.1016/j.jallcom.2009.09.024

[13] Qiu, J., Wang, Y. and Gu, M. (2006) *Materials Letters*, **60**, 2728. http://dx.doi.org/10.1016/j.matlet.2006.01.079

[14] Meaz, T.M. and Bender Koch, C. (2005) *Hyperfine Interactions*, **166**, 455. http://dx.doi.org/10.1007/s10751-006-9308-3

[15] Dhage, V.N., Mane, M.L., Babrekar, M.K., Kale, C.M. and Jadhav, K.M. (2011) *Journal of Alloys and Compounds*, **509**, 4394. http://dx.doi.org/10.1016/j.jallcom.2011.01.040

[16] Kreber, E. and Gonser, U. (1973) *Applied Physics*, **1**, 339. http://dx.doi.org/10.1007/BF00884403

[17] Shirtcliffe, N.J., Thompson, S., O'Keefe, E.S., Appleton, S. and Perry, C.C. (2007) *Mater. Res. Bull.*, **42**, 281. http://dx.doi.org/10.1016/j.materresbull.2006.06.001

[18] Bsoul, I., Mahmood, S.H. and Lehlooh, A.-F. (2010) *Journal of Alloys and Compounds*, **498**, 157. http://dx.doi.org/10.1016/j.jallcom.2010.03.142

[19] Tang, X., Yang, Y. and Hu, K.A. (2009) *Journal of Alloys and Compounds*, **477**, 488. http://dx.doi.org/10.1016/j.jallcom.2008.10.052

[20] Mendoza-Suárez, G., Rivas-Vázquez, L.P., Corral-Huacuz, J.C., Fuentes, A.F. and Escalante-García, J.I. (2003) *Materials Research Bulletin*, **339**, 110. http://dx.doi.org/10.1016/j.physb.2003.08.120

[21] Gao, X., Du, Y., Liu, X., Xu, P. and Han, X. (2011) Mater. Res. Bull., **46**, 643. http://dx.doi.org/10.1016/j.materresbull.2011.02.002

[22] Soman, V.V., Nanoti, V.M. and Kulkarni, D.K. (2013) *Ceramics International*, **39**, 5713. http://dx.doi.org/10.1016/j.ceramint.2012.12.089

[23] Venkateshwarlu, Ch., Ashok, Ch., Appa Rao, B., Ravinder, D. and Boyanov, B.S. (2006) *Journal of Alloys and Compounds*, **426**, 1. http://dx.doi.org/10.1016/j.jallcom.2006.02.001

[24] Topal, U. (2011) *Materials Science and Engineering*: *B*, **176**, 1531. http://dx.doi.org/10.1016/j.mseb.2011.09.019

[25] Du, Y., Gao, H., Liu, X., Wang, J., Xu, P. and Han, X. (2010) *Journal of Materials Science*, **45**, 2442. http://dx.doi.org/10.1007/s10853-010-4215-z

[26] Teh, G.B., Saravanan, N. and Jefferson, D.A. (2007) *Materials Chemistry and Physics*, **105**, 253. http://dx.doi.org/10.1016/j.matchemphys.2007.04.054

[27] Sözeri, H., Durmuş, Z., Baykal, A., Uysal, E. (2012) *Materials Science and Engineering*: *B*, **177**, 949.

[28] Martirosyan, K.S., Galstyan, E., Hossain, S.M., Wang, Y.-J. and Litvinov, D. (2011) *Materials Science and Engineering*: *B*, **176**, 8. http://dx.doi.org/10.1016/j.mseb.2010.08.005

[29] Tang, X., Zhao, B.Y. and Hu, K.A. (2006) *Journal of Materials Science*, **41**, 3867. http://dx.doi.org/10.1007/s10853-006-6676-7

[30] Han, M., Ou, Y., Chen, W. and Deng, L. (2009) *Journal of Alloys and Compounds*, **474**, 185. http://dx.doi.org/10.1016/j.jallcom.2008.06.047

[31] Iqbal, M.J., Ashiq, M.N. and Gomez, P.H. (2009) *Journal of Alloys and Compounds*, **478**, 736. http://dx.doi.org/10.1016/j.jallcom.2008.11.136

[32] Albanese, G. (1977) *Journal of Physics*, **38**, C1-85. http://dx.doi.org/10.1051/jphys:019770038010100

[33] Qiu, J., Lan, L., Zhang, H. and Gu, M. (2008) *Journal of Alloys and Compounds*, **453**, 261. http://dx.doi.org/10.1016/j.jallcom.2006.11.059

[34] González-Angeles, A., Lipka, J., Grusková, A., Jančárik, V., Tóth, I. and Sláma, J. (2008) *Hyperfine Interactions*, **184**, 135. http://dx.doi.org/10.1007/s10751-008-9778-6

[35] Bsoul, I., Mahmood, S.H., Lehlooh, A.-F. and Al-Jamel, A. (2013) *Journal of Alloys and Compounds*, **551**, 490. http://dx.doi.org/10.1016/j.jallcom.2012.11.062

[36] Lipka, J., Grusková, A., Orlicky, O., Sitek, J., Miglierini, M., Grone, R., Hucl, M. and Tóth, I. (1990) *Hyperfine Interactions*, **59**, 381. http://dx.doi.org/10.1007/BF02401253

[37] Kreber, E. and Gonser, U. (1976) *Applied Physics*, **10**, 175. http://dx.doi.org/10.1007/BF00896336

[38] Jacobo, S.E., Domingo-Pascual, C., Rodriguez-Clemente, R. and Blesa, M.A. (1997) *Journal of Materials Science*, **32**, 1025. http://dx.doi.org/10.1023/A:1018582423406

[39] Grusková, A., Sláma, J., Dosoudil, R., Kevická, D., Jančárik, V. and Tóth, I. (2002) *Journal of Magnetism and Magnetic Materials*, **242-245**, 423. http://dx.doi.org/10.1016/S0304-8853(01)01139-8

[40] Chen, Y.L., Li, X.D. and Xu, B.F. (1990) *Hyperfine Interactions*, **62**, 219. http://dx.doi.org/10.1007/BF02397701

[41] Evans, B.J., Grandjean, F., Lilot, A.P., Vogel, R.H. and Gérard, A. (1987) *Journal of Magnetism and Magnetic Materials*, **67**, 123. http://dx.doi.org/10.1016/0304-8853(87)90728-1

[42] Gao, F., Li, D. and Zhang, S. (2003) *Journal of Physics*: *Condensed Matter*, **15**, 5079. http://dx.doi.org/10.1088/0953-8984/15/29/319

[43] Meaz, T.M. and Bender, Koch C. (2004) *Hyperfine Interactions*, **156/157**, 341. http://dx.doi.org/10.1023/B:HYPE.0000043251.88839.a1

[44] Dushaq, G.H., Mahmood, S.H., Bsoul, I., Juwhari, H.K., Lahlouh, B. and AlDamen, M.A. (2013) *Acta Metallurgica*

Sinica, **26**, 509. http://dx.doi.org/10.1007/s40195-013-0075-2

[45] Warren, B.E. (1969) X-Ray Diffraction. Addison-Wesley, Reading, MA.

[46] Kaur, B., Bhat, M., Licci, F., Kumar, R., Kulkarni, S.D., Joy, P.A., Bamzai, K.K. and Kotru, P.N. (2006) *Journal of Magnetism and Magnetic Materials*, **305**, 392. http://dx.doi.org/10.1016/j.jmmm.2006.01.110

[47] González-Angeles, A., Mendoza-Suárez, G., Grusková, A., Papánová, M. and Sláma, J. (2005) *Materials Letters*, **59**, 26. http://dx.doi.org/10.1016/j.matlet.2004.09.012s

[48] Cullity, B.D. and Graham, C.D. (2009) Introduction to Magnetic Materials. Wiley, Hoboken, New Jersey.